SCIENTIFIC REPORTS

Tuned NV emission by in-plane Al-Schottky junctions on hydrogen terminated diamond

Christoph Schreyvogel[1], Marco Wolfer[1], Hiromitsu Kato[1,3], Matthias Schreck[2] & Christoph E. Nebel[1]

[1]Fraunhofer-Institute for Applied Solid State Physics, IAF, 79108 Freiburg, Germany, [2]Institute of Physics, University of Augsburg, 86159 Augsburg, Germany, [3]Energy Technology Research Institute, AIST, Tsukuba, Japan.

The negatively charged nitrogen-vacancy (NV) centre exhibits outstanding optical and spin properties and thus is very attractive for applications in quantum optics. Up to now an active control of the charge state of near-surface NV centres is difficult and the centres switch in an uncontrolled way between different charge states. In this work, we demonstrate an active control of the charge state of NV centres (implanted 7 nm below the surface) by using an in-plane Schottky diode geometry from aluminium on hydrogen terminated diamond in combination with confocal micro-photoluminescence measurements. The partial quenching of NV-photoluminescence caused by the hole accumulation layer of the hydrogen terminated surface can be recovered by applying reverse bias potentials on this diode, i.e. the NV^0 charge state is depleted while the NV^- charge state is populated. This charge state conversion is caused by the bias voltage affected modulation of the band bending in the depletion region which shifts the Fermi level across the NV charge transition levels.

The nitrogen-vacancy (NV) centre in diamond has attracted significant interest over recent years as it is promising for applications in quantum information processing[1–4], single-spin magnetometry[5,6] and plasmonics[7,8]. One of the outstanding properties is that the spin of the negatively charged NV centre can be initialized and read-out optically[9].

For most of the applications, it is essential to use NV^- defects as close as possible to the diamond surface (1–10 nm below the surface), either to enhance the sensitivity of diamond-based magnetic sensors or to efficiently couple the emitted photoluminescence to a photonic waveguide or a microcavity[10,11]. However, the charge state of near-surface NV centres is strongly affected by surface defects, surface terminations and adsorbates and switches in an uncontrolled way between NV^-, NV^0 and presumably NV^+ [12–17]. The control over the charge state of the NV centre is difficult up to now. A prerequisite would be to control the position of the Fermi level within the bandgap. Passive control is achieved by surface termination with oxygen[15–17] and active control has recently been achieved by using a solution-gated field effect transistor[18]. Recently, H. Kato and co-workers demonstrated an active control of the charge state of NV centres in the intrinsic layer of a diamond-based pin-diode[19]. With this three-dimensional device a switching of the NV charge state could be achieved from NV^- to NV^0.

In this work, we use a two-dimensional Schottky junction of aluminium on hydrogen terminated diamond[20,21]. Aluminium forms a Schottky contact on H-terminated diamond inducing a lateral hole depletion layer next to the Al contact. By applying external potentials to the Al contact the band bending in the depletion region can be manipulated. As a consequence, the Fermi level shifts in such a way that the charge state of NV centres is switched. Using confocal micro-photoluminescence we demonstrate an increasing depletion of the NV^0 charge state and population of the NV^- charge state with increasing reverse bias voltages applied to this diode.

Results

Experiments were performed on a 300 μm thick ultra-pure diamond grown homoepitaxially on Ib substrate by Microwave Plasma-Enhanced Chemical Vapour Deposition (MWPECVD)[22]. After growth the sample was wet-chemically cleaned and oxidized.

For photoluminescence characterizations we used a confocal microscope with an excitation wavelength of 532 nm. All presented spectra were normalised to the intensity of the first order Raman line of diamond. Please note that only spectra acquired with the same excitation and detection conditions are compared in each figure.
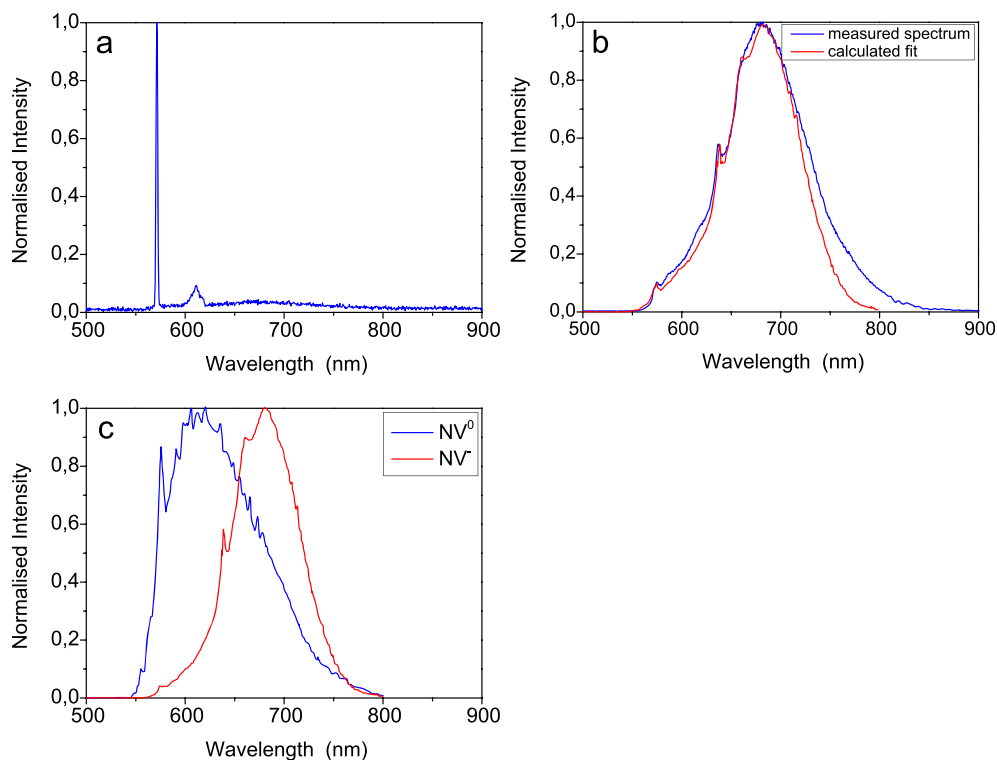
Figure 1 | Formation of NV centres. (a) Photoluminescence spectrum of the grown diamond epi-layer with oxidized surface, normalized to the first order Raman line. The first and second order Raman lines as well as a weak NV signal are visible. The latter originates from the substrate containing a high nitrogen concentration. (b) NV-Photoluminescence spectrum (blue line) after nitrogen ion-beam implantation and annealing. The spectrum, normalized to the maximum intensity of the NV^- phonon side bands, shows typical features such as the zero phonon line of the neutral charge state NV^0 at 2.156 eV (575 nm) and of NV^- at 1.945 eV (637 nm) and their phonon sidebands. The red curve is the weighted superposition of single NV^0 and NV^- spectra (see Fig. c) fitted to the measured spectrum for calculation of the NV^0 to NV^- ratio. (c) Normalized photoluminescence spectra of single NV^0 and NV^- centres as measured by Rondin *et al.*[15].

The confocal micro-photoluminescence (µPL) spectrum of the grown diamond epi-layer with oxidized surface, shown in Fig. 1a, is dominated by the first and second order Raman lines as well as low NV signal. The latter originates from the Ib substrate containing a high nitrogen concentration.

In the next step, nitrogen ions with a dose of 10^{13} ions/cm^2 have been implanted at an average depth of 7 nm (5 keV implantation energy)[17,23] covering homogeneously the whole diamond sample area. In order to activate the diffusion of vacancies to produce NV centres, the sample was annealed at 800°C. The efficiency of this formation process is about 1–10%[24], resulting in an NV centre sheet density of about 10^{12} cm^{-2} and NV emission as shown in Fig. 1b. To analyse the proportion of NV^0 and NV^- luminescence, a weighted superposition of pure NV^0 and NV^- emission spectra (Fig. 1c) as published in literature[15] was fitted to the measured spectrum in Fig. 1b (details are described in the methods section). The fit revealed that 10% of the total spectrum results from NV^0 and 90% from NV^-.

After implantation and annealing, the surface was hydrogen (H)-terminated. The hydrogen termination quenched the NV-PL by roughly 50% as shown in Fig. 2. Furthermore, after H-termination the composition of the NV emission is changed to 20% of NV^0 and 80% of NV^-.

To control the charge state of NV centres, we fabricated an in-plane Schottky diode, which is schematically shown in Fig. 3a. Aluminium (Al) was used as Schottky metal showing a barrier height of about 570 meV and gold (Au) as an ohmic contact[20,21]. The IV-characteristic of the fabricated in-plane Schottky diode measured at ambient conditions is shown in Fig. 3b. An on/off ratio of more than 7 orders of magnitude is achieved.

To investigate the influence of external bias voltages on the NV emission, originating from NV centres in the depletion region next to the Al contact, we used a long working distance objective to avoid short circuits between the microscope objective and the metallized and wired diamond surface.

The results of the µPL measurements performed at the edge of the Al contact (spot 1 in Fig. 3a) for different reverse bias voltages are shown in Fig. 4a. Each spectrum was normalized to the amplitude of the first order Raman line to enable a direct comparison and a quantitative evaluation comparison and evaluation. With increasing reverse bias voltage the intensity of the NV^- part of the spectrum increases, while the NV^0 part decreases. The absolute NV^- emission is increased by 20% – 30%. We also performed spectral
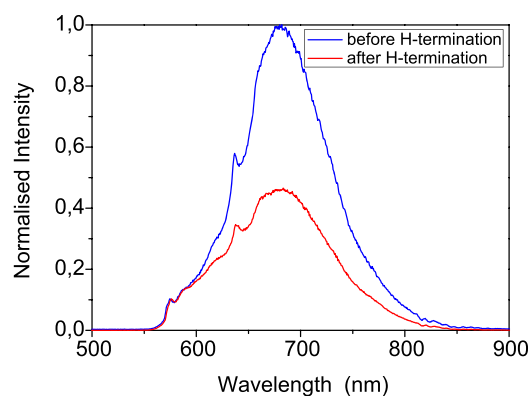

Figure 2 | Quenching of NV emission. NV spectra measured before and after hydrogen-termination. After H-termination, the intensity of the NV emission is quenched partially. The spectra are normalized to the first order Raman line.
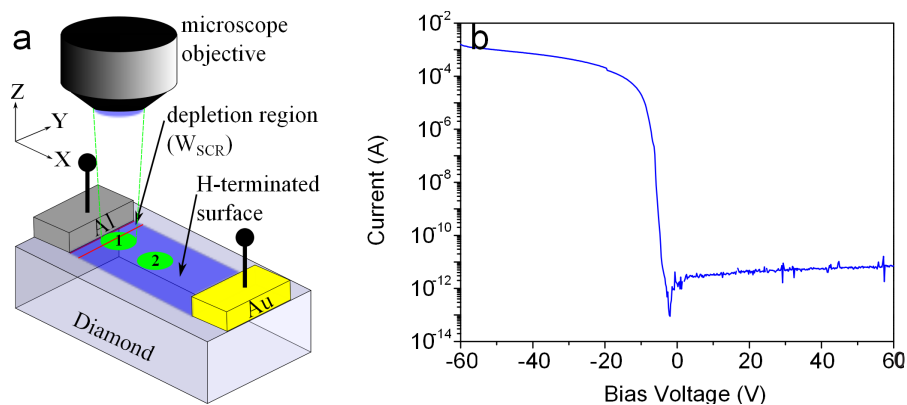
Figure 3 | In-plane Schottky diode from diamond. (a) Schematic figure of an in-plane Al Schottky diode on H-terminated diamond surface. A confocal μPL measurement was performed at the edge of the Al contact (green spot 1) to investigate the bias-voltage dependent variation of NV emission in the depletion region. The reference spectrum was measured 100 μm away from the edge of the Al contact (green spot 2). (b) The current-voltage properties of the fabricated in-plane Al-Schottky diode measured at ambient conditions at T = 300 K.

measurements under forward bias conditions but we could neither detect any change in the spectra nor observed electroluminescence from NV centres.

The spectra in Fig. 4a contain a high background originating from NV centres outside the depletion region (see discussion section for explanation) and from the substrate. As the Fermi level in the area outside the depletion region is not altered by the bias voltage, the NV-PL from that region is constant. It has been measured ca. 100 μm away from the depletion region (indicated as spot 2 in Fig. 3a) and is shown in Fig. 4b. This reference spectrum was subtracted from the bias voltage affected spectra in Fig. 4a. As a result we get the relative change of the NV-PL intensities for different bias-voltages. The obtained data plotted in Fig. 4c show that the NV$^-$ signal is enhanced

and the NV^0 emission is reduced. In addition, we calculated the relative change of the integrated intensities of the NV^0 and NV$^-$ amplitudes in Fig. 4c at different bias-voltages. The integrated intensity of the NV$^-$ amplitude increases approximately by a factor of 10 and the NV^0 amplitude decreases just approximately by a factor of 4 (Fig. 4d).

The features shown in Figs. 4a,c and d are reproducibly measured at different positions along the Al-contact. This is a strong support for the interpretation of the spectral changes in terms of af field-induced variation of the charge-state of NV centres.

It should also be noted that the intensity of the first order Raman line in the μPL spectra in Figs. 1b and 2 is much lower than that shown in Figs. 4a and 4b. This change in Raman intensity is a simple
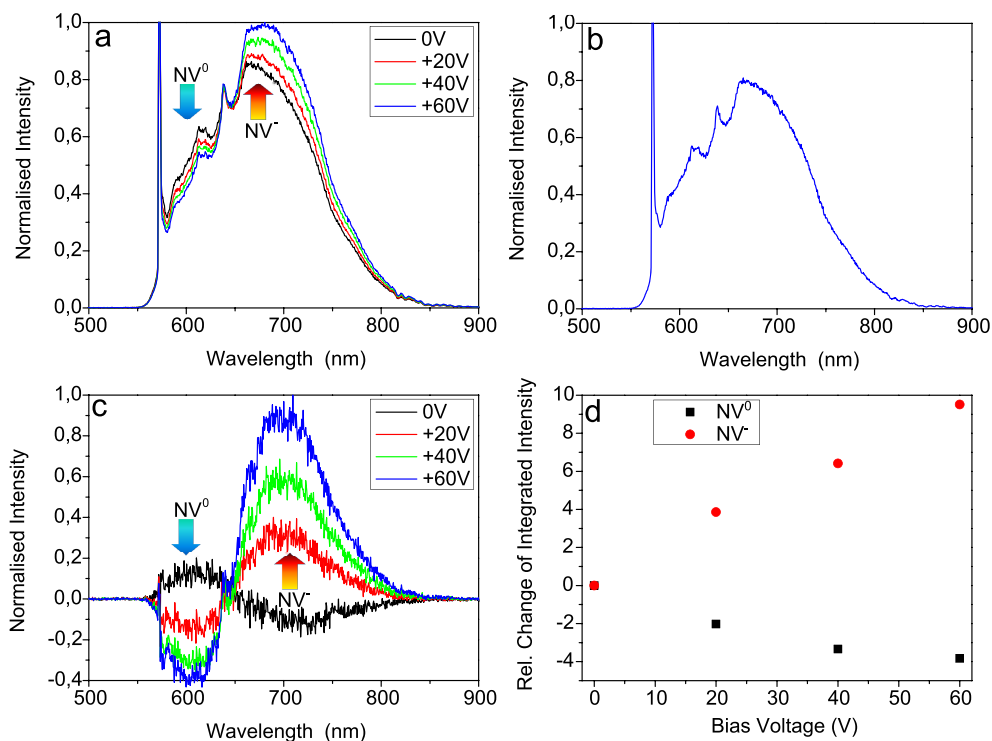

Figure 4 | Tuned NV emission. (a) Variation of the NV spectra for different reverse bias potentials (measured on spot 1 depicted in Fig. 3a). Each spectrum was normalized to the amplitude of the first order Raman line to allow comparison and evaluation. (b) Reference spectrum (normalized to the first order Raman line) measured on spot 2 as depicted in Fig. 3a. (c) Background corrected variations of the spectra shown in (a) with the amplitudes normalized to the maximum amplitude. (d) Relative change of the integrated intensities of the NV^0 and NV$^-$ amplitudes in (c) for different bias-voltages applied.
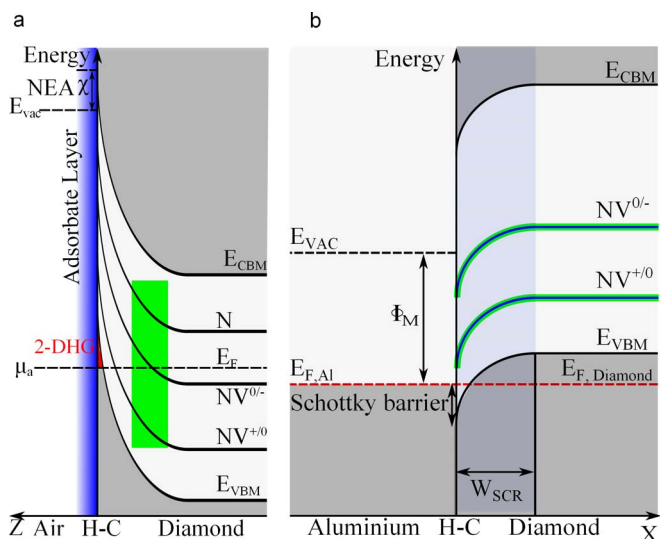
Figure 5 | Formation of an in-plane Schottky junction. (a) Schematic of the energy band diagram of an H-terminated diamond from the surface into the bulk (z-axis as depicted in Fig. 3a). E_{vac} is the vacuum level, χ is the negative electron affinity, E_{VBM} and E_{CBM} is the valence band maximum and the conduction band minimum respectively, E_F is the Fermi level. H-C indicates the carbon-hydrogen bond at the surface and μ_a is the chemical potential of the aqueous wetting layer covering the diamond surface. 2-DHG is the two-dimensional p-type channel. Also shown are the charge transition levels $NV^{+/0}$ (1.2 eV above valence band maximum E_{VBM}[29]) and $NV^{0/-}$ (2.8 eV above valence band maximum E_{VBM}[18]) as well as the nitrogen donor level N (1.7 eV below conduction band minimum E_{CBM}[30]). The green square indicates the region below the surface covered by nitrogen and both NV^- and NV^0 centres generated by implantation (centre position is 7 nm below the surface with a standard deviation of 2.3 nm). (b) Schematic lateral band diagram of the Al/H-terminated diamond interface (x-axis as depicted in Fig. 3a). Φ_M is the work function of Al and w_{SCR} is the width of the lateral depletion region. The green lines at the NV charge transition levels indicate the NV-layer region. The energy level N of nitrogen, as shown in a), is not displayed for a better overview.

measurement artefact[25] resulting from the application of a long working distance objective with a lower numerical aperture in the latter experiment.

Discussion

To understand the partial quenching of the NV-photoluminescence after H-termination of the surface (Fig. 2), the band bending at the diamond surface need to be considered which is shown schematically in Fig. 5a and explained in the following. Hydrogen terminated diamond shows a negative electron affinity χ[26–28]. Therefore, the chemical potential μ_a of the aqueous wetting layer covering the diamond surface is below the valence band maximum giving rise to tunnelling of electrons from the valence band into the lowest unoccupied electronic states of the adsorbate film (transfer doping model)[27,28]. This induces a band bending from the surface into the bulk and the formation of a two-dimensional hole accumulation layer at the diamond surface with a typical hole sheet density of $N = 10^{12}$ cm^{-2} [27,28]. Calculations by Nebel *et al.*[28] show that this hole accumulation layer extends approximately 1–4 nm into the diamond bulk. The charge transition level is defined as a level at which a defect centre takes up or loses an electron when the Fermi level crosses this level. Towards the surface, the NV charge transition levels $NV^{+/0}$ (1.2 eV above valence band maximum[29]) and $NV^{0/-}$ (2.8 eV above valence band maximum[18]) are moving above the Fermi level as schematically shown in Fig. 5a. As both charge transition levels are unoccupied the NV photoluminescence is quenched. With an average implantation

depth of 7 nm the NV enriched layer is spatially separated from the hole accumulation layer which is also shown in Fig. 5a. However, the observed partial quenching can be explained by tunnelling transitions from the nearby hole channel and by the fact that the sheet density of implanted nitrogen ions of 10^{13} cm^{-2} exceeds the typical hole sheet density of just 10^{12} cm^{-2}. It should be mentioned that the hole sheet density is determined by the quality of the H-termination and by the diamond surface roughness. Typical values for the hole sheet density are varying between 5×10^{11} and 5×10^{12} cm^{-2} [21].

For the interpretation of the bias-dependent NV emission, the formation and the working principle of the two-dimensional Schottky junction at the Al/H-terminated diamond interface need to be considered. The work function of Al is smaller than that of an H-terminated diamond surface, thus a Schottky barrier for holes in the two-dimensional p-type surface conductive layer is induced[21]. As a result, a lateral hole depletion region next to the Al contact is formed as schematically shown in Fig. 5b. The NV charge transition levels $NV^{+/0}$ and $NV^{0/-}$ are also displayed in the lateral band diagram in Fig. 5b. Please note that the NV centres are homogeneously distributed between the Al and the Au contact, following the band bending of the Schottky contact as schematically shown in Fig. 5b.

The width w_{SCR} of the depletion layer can be estimated[21]:

$$w_{SCR} \propto \frac{\varepsilon_0 \varepsilon_r}{2\pi e} \frac{V}{p_{sh}},$$

where ε_0 is the vacuum permittivity, ε_r is the relative permittivity of diamond, e is the elementary charge, V is the applied reverse voltage and p_{sh} is the hole sheet density which is typically about 10^{12} cm^{-2} [21]. For reverse voltages between V = 3 and 60 V, the estimated depletion layer width varies between 15 nm and 300 nm. As we use a long working distance objective of NA = 0.5 and an excitation wavelength of $\lambda_{exc} = 532$ nm, the calculated lateral resolution $r_{lat} = 0.4\lambda_{exc}/NA$ of the confocal measurement is about 426 nm. Due to this, the laser-illuminated area is (especially for small reverse bias voltages) much larger than the depletion layer which is schematically indicated in Fig. 3a. Therefore, only a small fraction of the NV centres addressed by the confocal µPL measurement is located within the depletion layer and only these centres produce the change in the µPL spectra if a reverse bias voltage is applied on Al contact resulting in a moderate signal modulation of the NV spectrum (see Fig. 4a).

The change of the µPL spectra for different reverse bias voltages (Fig. 4a) can be interpreted by taking the band bending modulation in the depletion region of the in-plane Schottky junction into consideration which is shown schematically in Figs. 6 a and b. By increasing the reverse bias voltage, the Fermi-level in the depletion region first crosses the $NV^{+/0}$ and then the $NV^{0/-}$ transition level (Fig. 6a). In this way, non-fluorescent NV^+ centres switch to NV^0 while NV^0 centres closer to the aluminium contact switch to NV^-. Thus, we would expect an increase of NV^- emission with increasing reverse bias. The smaller change of the NV^0 emission (Fig. 4d) is most likely due to fact that an NV^+ to NV^0 conversion takes place which thus minimizes the decrease of NV^0 emission. By applying forward potentials we expect the opposite, i.e. the Fermi-level is pushed below the $NV^{+/0}$ transition level and thus the NV centres are switched to the non-fluorescent state NV^+. An overall decrease of the NV-PL intensity could not be observed in our experiment due to the very small depletion layer width which even becomes smaller or even vanishes by applying increasing forward potentials. Thus, the spectra are dominated strongly by NV emission next to the depletion region and the variation of the total spectrum upon applying forward voltages will be below the detection limit.

In summary, we have shown for the first time that the charge state of the NV centre can be manipulated in the depletion region of an in-plane Al Schottky junction. Application of reverse bias voltages resulted in conversion from NV^0 to NV^-. If the charging and
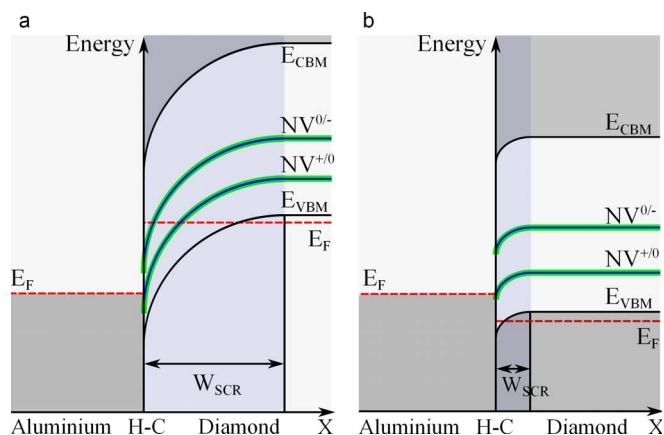
Figure 6 | Working principle of an in-plane Schottky junction. Schematic band-diagram of a Schottky-junction for (a) reverse bias and (b) forward bias voltages applied on Al-Schottky contact. The green lines at the NV charge transition levels indicate the NV-layer region. For reverse bias voltages applied on Schottky contact the Fermi-level E_F is pushed towards the $NV^{0/-}$ level, resulting in an increase of NV^- emission close to the Al contact. For forward bias-voltages, the Fermi-level E_F is pushed below the $NV^{+/0}$ transition level and thus the NV centres are switched to the non-fluorescent state NV^+.

discharging would be governed by tunnelling transitions to the Al metal contact we expect fast switching behaviour. In addition to that, this planar diode structure can be easily integrated into quantum optical devices such as quantum registers which then enables the electron spins of the NV centres to be switched on and off on demand and thus allow or block the optical manipulation of the spins.

In the present experiments the density of implanted NV centres was too high to detect single centres by confocal μPL. We are currently preparing new experiments with nitrogen-implantation densities around 10^8 cm^{-2} to characterise properties of single NV centres in the close vicinity of Al-Schottky contacts.

Methods

Fabrication of in-plane Schottky diode from diamond with NV centres. For realizing a two-dimensional Schottky-diode we prepared a diamond sample. An Ib (001) $3 \times 3 \times 0.5$ mm diamond plate from Element Six Ltd. was used as substrate and a 300 μm thick intrinsic, nitrogen free epi-layer was grown homoepitaxially onto this substrate using the ellipsoidal shaped MWPECVD (Microwave Plasma-enhanced Chemical Vapour Deposition) reactor[20]. The process parameters used were 200 mbar gas pressure at a gas flow of 400 sccm H_2 and 16 sccm CH_4 (which corresponds to a CH_4/H_2 ratio of 4%), 0.5 sccm O_2 and a microwave power of 4.5 kW. Under these conditions, the measured growth temperature was about 780°C. The growth rate was 2.1 μm/h.

A shallow nitrogen-ion beam implantation, with implantation energy of 5 keV and a sheet density of $N = 10^{13}$ cm^{-2}, was applied to realize an NV-layer close to the surface. The resulting implantation profile shows a Gaussian density distribution with a centre position of 7 nm (1.4 nm/keV) and a standard deviation of 2.3 nm (0.46 nm/keV) that has been simulated with the software SRIM (stopping and range of ions in matter)[17,23]. The formation of NV centres was achieved by annealing the sample for 1 h at 800°C.

Hydrogen termination was achieved by applying pure hydrogen plasma in the MWPECVD reactor at a pressure of 100 mbar, with a microwave power of 1.9 kW. The duration of the termination process was 1 minute at a temperature of around 500°C.

The fabrication of the in-plane Schottky diode was realized by using photolithography in combination with thermal evaporation of Al and Au with a thickness of 50 nm each on the diamond surface. The contacts were 500 μm × 500 μm large and separated from each other by a distance of 500 μm.

Experimental setup for optical detection. Our confocal microscope set-up is equipped with a diode-pumped and frequency-doubled Nd:YAG-laser operating at a wavelength of 532 nm with an output power of 5 mW and a commercial confocal microscope (LabRam BX41, Horiba Jobin Yvon). The laser beam is passed to the microscope through an optical fibre and focused onto the sample by the microscope objective. The laser power illuminating the sample is 1 mW due to losses in the optical path of the microscope setup. The resulting photoluminescence signal is collected by

the same objective and the excitation wavelength is spectrally filtered out using notch filter. The light beam is subsequently focused onto a pinhole for spatial filtering and routed via a fibre to a monochromator (iHR-320, Horiba Jobin Yvon). As detector a Peltier-cooled CCD-Camera (SYNAPSE, Horiba Jobin Yvon) was used.

To investigate the tuned NV emission, we used an objective with a long working distance (Olympus LMPlanFLN, 50×, NA = 0.5, WD = 10.6 mm) to avoid a short circuit between the microscope objective and the metallized and wired diamond surface.

1. Weber, J. R. *et al.* Quantum computing with defects. *Proc. Natl. Acad. Sci. USA* **107**, 8513–8518 (2010).
2. Balasubramanian, G. *et al.* Ultralong spin coherence time in isotopically engineered diamond. *Nat. Mater.* **8**, 383–387 (2009).
3. Neumann, P. *et al.* Quantum register based on coupled electron spins in a room-temperature solid. *Nat. Phys.* **6**, 249–253 (2010).
4. Neumann, P. *et al.* Single-Shot Readout of a Single Nuclear Spin. *Science* **329**, 542–544 (2010).
5. Maze, J. R. *et al.* Nanoscale magnetic sensing with an individual electronic spin in diamond. *Nature* **455**, 644–648 (2008).
6. Balasubramanian, G. *et al.* Nanoscale imaging magnetometry with diamond spins under ambient conditions. *Nature* **455**, 649–652 (2008).
7. Kolesov, R. *et al.* Wave-particle duality of single surface plasmon polaritons. *Nat. Phys.* **5**, 470–474 (2009).
8. Schietinger, S. *et al.* Plasmon-enhanced single photon emission from a nanoassembled metal-diamond hybrid structure at room temperature. *Nano Lett.* **9**, 1694–1698 (2009).
9. Jelezko, F. & Wrachtrup, J. Read-out of single-spins by optical spectroscopy. *J. Phys.: Condens. Matter* **16**, R1089–R1104 (2004).
10. Barth, M., Nüsse, N., Löchel, B. & Benson, O. Controlled coupling of a single-diamond nanocrystal to a photonic crystal cavity. *Opt. Lett.* **34**, 1108–1110 (2009).
11. Barclay, P. E., Fu, K. M. C., Santori, C. & Beausoleil, R. G. Chip-based microcavities coupled to NV centers in single crystal diamond. *Appl. Phys. Lett.* **95**, 191115 (2009).
12. Gaebel, T. *et al.* Photochromism in single nitrogen-vacancy defect in diamond. *Appl. Phys. B-Lasers O* **82**, 243–246 (2006).
13. Manson, N. B. & Harrison, J. P. Photo-ionization of the nitrogen-vacancy center in diamond. *Diam. Relat. Mater.* **14**, 1705–1710 (2005).
14. Waldherr, G. *et al.* Dark States of Single Nitrogen-Vacancy Centers in Diamond Unraveled by Single Shot NMR. *Phys. Rev. Lett.* **106**, 157601 (2011).
15. Rondin, L. *et al.* Surface-induced charge state conversion of nitrogen-vacancy defects in nanodiamonds. *Phys. Rev. B* **82**, 115449 (2010).
16. Fu, K. M. C., Santori, C., Barclay, P. E. & Beausoleil, R. G. Conversion of neutral nitrogen-vacancy centers to negatively charged nitrogen-vacancy centers through selective oxidation. *Appl. Phys. Lett.* **96**, 121907 (2010).
17. Hauf, M. V. *et al.* Chemical control of the charge state of nitrogen-vacancy centers in diamond. *Phys. Rev. B* **83**, 081304(R) (2011).
18. Grotz, B. *et al.* Charge state manipulation of qubits in diamond. *Nat. Commun.* **3**, 729 (2012).
19. Kato, H., Wolfer, M., Schreyvogel, C., Kunzer, M. & Müller-Sebert, W. Tunable light emission from nitrogen-vacancy centers in single crystal diamond PIN diodes. *Appl. Phys. Lett.* **102**, 151101 (2013).
20. Nebel, C. E. *et al.* Electrochemical properties of undoped diamond. In *Physics and Applications of CVD diamond*, Editors Koizumi, S., Nebel, C. E. & Nesladek, M. (Wiley-VCH, 2008).
21. Nebel, C. E., Rezek, B., Shin, D. & Watanabe, H. Surface electronic properties of H-terminated diamond in contact with adsorbates and electrolyte. *Phys. Stat. Sol. (a)* **203**, 3273–3298 (2006).
22. Füner, M., Wild, C. & Koidl, P. Novel microwave plasma reactor for diamond synthesis. *Appl. Phys. Lett.* **72**, 1149–1151 (1998).
23. Ziegler, J. F., Ziegler, M. D. & Biersack, J. P. SRIM - the stopping and range of ions in matter (2010). *Nucl. Instrum. Meth. B* **268**, 1818–1823 (2010).
24. Acosta, V. M. *et al.* Diamonds with a high density of nitrogen-vacancy centers for magnetometry. *Phys. Rev. B* **80**, 115202 (2009).
25. Webb, R. H. Confocal optical microscopy. *Rep. Prog. Phys.* **59**, 427–471 (1996).
26. Takeuchi, D. *et al.* Direct observation of negative electron affinity in hydrogen-terminated diamond surface. *Appl. Phys. Lett.* **86**, 152103 (2005).
27. Nebel, C. E. *et al.* Electronic properties of the 2D-hole accumulation layer on hydrogen terminated diamond. *Diam. Relat. Mater.* **13**, 2031–2036 (2004).
28. Nebel, C. E. *et al.* 2D-hole accumulation layer in hydrogen terminated diamond. *Phys. Stat. Sol. (a)* **201**, No. 11 , 2432–2438 (2004).
29. Goss, J. P., Briddon, P. R., Jones, R., Sque, S. & Rayson, M. J. Vacancy-impurity complexes and limitations for implantation doping of diamond. *Phys. Rev. B* **72**, 035214 (2005).
30. Collins, A. T. The Fermi level in diamond. *J. Phys.: Condens. Matter* **14**, 3743–3750 (2002).

Acknowledgments

Author contributions

C.S. contributed as first author, fabricated the in-plane Schottky junction on H-terminated diamond surface and performed the experiments and analysed the data. H.K. performed the sample growth and M.S. the nitrogen-ion beam implantation. M.W. was in charge for the confocal micro-PL experiments and C.E.N. stimulated and supervised the research activity.

Additional information

Competing financial interests: The authors declare no competing financial interests.